Silica Gels with Tunable Nanopores through Templating of the L₃ Phase

K. M. McGrath,[†] D. M. Dabbs,[‡,§] N. Yao,[§] K. J. Edler,[∥] I. A. Aksay,*[,‡,§] and
S. M. Gruner[∥]

*Chemistry Department, University of Otago, Dunedin, New Zealand, Department of
Chemical Engineering and Princeton Materials Institute, Princeton University,
Princeton, New Jersey 08544-5263, and Physics Department, Cornell University,
Ithaca, New York 14853-2501*

We describe a detailed synthesis of a silicified inorganic/organic nanoporous monolithic composite conforming to the lyotropic liquid crystalline L₃ phase. The pore dimensions of the silicified L₃ phase scale with the solvent volume fraction in the synthesis reaction mixture. Changing the solvent fraction in the initial solution changes the ultimate pore diameter in the silicate, providing a simple method for tuning the diameter of the pores in the matrix. The resulting monolith is optically isotropic and transparent with a nonperiodic network. Accessible pores (which permeate the entire structure) in the silicified materials correlate with the solvent domain of the original liquid crystalline phase and therefore negate the need to remove the surfactant in order to gain access to the pore network. Measured characteristic dimensions are from 6 to well over 35 nm. X-ray scattering studies indicate a low polydispersity in the pore diameters for a given solvent fraction. Transmission electron and atomic force microscope images are consistent with a random morphology and measured surface areas exceed 960 m² g⁻¹ in extracted materials.

Introduction

The development of mesostructured materials[1,2] has led to considerable focus on the formation of mesoporous materials.[3] This is in part due to the large gap that exists between the respective length scales for synthesized structures and natural materials and also because mesoporous materials are seen to have high potential for applications over a wide range of material needs. Possible areas of use include filtration and prefiltration,[4,5] biological separation with fine molecular weight cutoff (as for DNA separation),[6] thin film pattern formation for use in optoelectronics,[7,8] catalyst and catalyst supports,[3] high molecular weight osmotic membranes,[6] heavy metal removal,[9,10] and as a matrix phase for the fabrication of composites.[11]

In their pioneering work, Beck et al.[2] synthesized a group of inorganic materials which conformed to the topological forms of hexagonal, bicontinuous cubic, and lamellar liquid crystalline phases of amphiphilic molecules, with pore dimensions of approximately 4 nm obtained after removing the amphiphilic molecules from the matrix. Due to the low concentrations of amphiphile in solution, a coassembly mechanism was proposed to explain the formation of higher order topologies not normally associated with low amphiphile concentrations.[1–5]

Alternatively, by working in the concentration domains correlating to the native hexagonal, bicontinuous cubic, and lamellar liquid crystalline phases in a nonionic/water system, Attard et al.[12,13] have produced monolithic inorganic materials whose structure mirrored the original geometry of the amphiphile. Their mechanism was closer to templating than coassembly. The methodology was limited in the pore dimensions obtainable. An additional problem was the necessity for continuous removal of byproduct (and only the byproduct) during synthesis to maintain the integrity of the phase.

These surfactant-formed mesostructures are usually limited by the maximum template size obtainable, the necessity of removing the amphiphilic material to gain access to the pores once polymerization of the inorganic material has occurred, and the lack of predictive control over product topologies. To overcome these difficulties, we chose to template a continuous liquid crystalline phase as recently demonstrated in the formation of a mesoporous, continuous pore structure using a bilayer, bicontinuous liquid crystal as a template onto which silica has been deposited.[14] These materials have pore surface areas comparable to those of aerogels (400–1000 m² g⁻¹) but with a high degree of uniformity in the pore size distribution and a highly connected, isotropic network structure which is mechanically more robust than those of typical

[†] Chemistry Department, University of Otago.

[‡] Department of Chemical Engineering, Princeton University.

[§] Princeton Materials Institute, Princeton University.

[∥] Physics Department, Cornell University.

(1) Kresge, C. T.; Leonowicz, M. E.; Roth, W. J.; Vartuli, J. C.; Beck, J. S. *Nature* **1992**, *359*, 710–12.

(2) Beck, J. S.; Vartuli, J. C.; Roth, W. J.; Leonowicz, M. E.; Kresge, C. T.; Schmitt, K. D.; Chu, C. T.-W.; Olson, D. H.; Sheppard, E. W.; McCullen, S. B.; Higgins, J. B.; Schlender, J. L. *J. Am. Chem. Soc.* **1992**, *114*, 10834–10843.

(3) Maschmeyer, T. *Curr. Opin. Solid State Mater. Sci.* **1998**, *3*, 71–8.

(4) Beck, J. S.; Vartuli, J. C.; Kennedy, G. J.; Kresge, C. T.; Roth, W. J.; Schramm, S. E. *Chem. Mater.* **1994**, *6*, 1816–21.

(5) Vartuli, J. C.; Schmitt, K. D.; Kresge, C. T.; Roth, W. J.; Leonowicz, M. E.; McCullen, S. B.; Hellring, S. D.; Beck, J. S.; Schlenker, J. L.; Olson, D. H.; Sheppard, E. W. *Chem. Mater.* **1994**, *6*, 2317–26.

(6) Davis, M. E. *Nature* **1993**, *364*, 391–3.

(7) Beecroft, L. L.; Ober, C. K. *Chem. Mater.* **1997**, *9*, 1302–17.

(8) Honma, I.; Zhou, H. S. *Chem. Mater.* **1998**, *10* (1), 103–8.

(9) Feng, X.; Fryxell, G. E.; Wang, L.-Q.; Kim, A. Y.; Liu, J.; Kemner, K. M. *Science* **1997**, *276*, 923–6.

(10) Mercier, L.; Pinnavaia, T. J. *Adv. Mater.* **1997**, *9* (6), 500–3.

(11) Ozin, G. A.; Chomski, E.; Khushalani, D.; MacLachlan, M. J. *Curr. Opin. Colloid Interface Sci.* **1998**, *3*, 181–93.

(12) Attard, G. S.; Glyde, J. C.; Göltner, C. G. *Nature* **1995**, *378*, 366–8.

(13) Attard, G. S.; Edgar, M.; Emsley, J. W.; Göltner, C. G. *Mater. Res. Soc. Symp. Proc.* **1996**, *425*, 179–84.

(14) McGrath, K. M.; Dabbs, D. M.; Yao, N.; Aksay, I. A.; Gruner, S. M. *Science* **1997**, *277*, 552–556; **1998**, *279*, 1289.
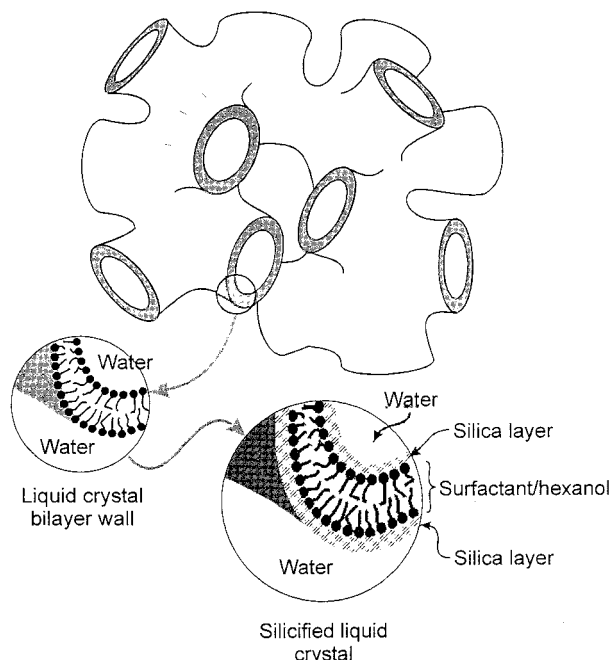
Figure 1. Schematic of the L_3 phase with a model of the silicification process.

Figure 2. CpCl phase diagram (from ref 18).

aerogels. Advantages of this system include the low concentration of organic phase within the matrix, the uniformity and accessibility of the pore structure, and control of the pore diameter. Our goals were to fabricate optically isotropic and transparent monoliths and nanoporous inorganics of low density and refractive index, while maintaining a well-defined, contiguous three-dimensional topology and fixed pore dimensions. In this paper, we detail the processing of the mesostructured silica and provide more evidence for the replication of the liquid crystal by silicification of the organic.

The L_3 phase is formed via self-assembly of amphiphiles with properties which make it an appropriate choice for use as a template in the formation of mesoporous inorganic materials. The phase consists of a three-dimensional random packing of a multiply connected continuous membrane,[15-17] which evenly sub-divides the solvent into two continuous volumes (Figure 1). The average pore and cavity dimensions of the water domains are controlled by the solvent volume fraction, varying from 1 to 100 nm, and the pore network permeates the entire structure.

The pore diameter in the L_3 increases with increasing solvent content, providing a procedure by which the pore diameter can be tuned to a specific size. The fine control achievable through control of solvent content leads to a very low pore size distribution for a given solvent volume fraction. In addition, the L_3 phase is optically isotropic and water clear, both properties which could be advantageous in a matrix or final composite. The L_3 phase has a viscosity comparable to that of water, which eases addition of inorganic precursors, often a problem in the more viscous hexagonal, bicontinuous cubic, and lamellar phases.

Figure 2 shows a slice through the quasiternary phase diagram for the 1-hexadecylpyridinium chloride (CpCl)/hexanol/brine (1 wt % NaCl in water) system used in our study, which forms the L_3 phase.[18] The phase is pure within
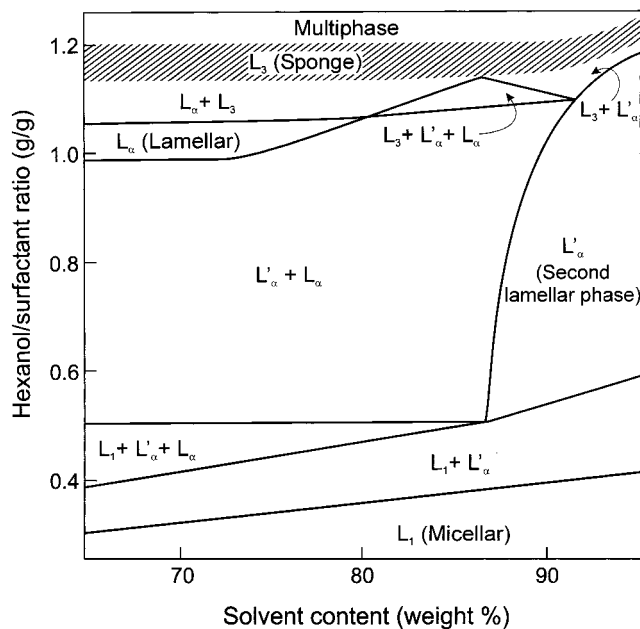
the domains of 53 to >98 wt % solvent and for hexanol to CpCl ratios of 1.12−1.21. The L_3 phase is bordered, in this slice of the phase diagram, by the lamellar phase (an indefinite stacking of bilayers intercalated with water) on one side (the lower hexanol composition side) and a multiphase region containing reverse micelles on the other. Both the composition of solvent and the ratio between the surfactant (CpCl) and the cosurfactant (in this case hexanol) maybe used to manipulate the phase. The L_3 phase Gaussian curvature is globally negative (i.e., the interface between aqueous and nonaqueous regions bends away from the hydrocarbon chains of the amphiphile). Locally, however, the curvature varies from being flat (Gaussian curvature = 0, "lamellar-like" stacking) to a minimum in the Gaussian curvature.

CpCl membranes without hexanol have too high a rigidity to allow the thermally driven variation in curvature required for the L_3 phase. The short hydrocarbon chain and small hydrophilic hydroxyl group of hexanol lower the membrane rigidity by virtue of its placement in the membrane bilayer, thereby facilitating the formation of the L_3 phase. This occurs over a very small range of hexanol to CpCl concentrations; adding an excessive amount of hexanol will cause a phase transition. The new phase has a close to uniform negative Gaussian curvature over the entire membrane. If too little hexanol is present in the solution for the formation of the L_3 phase, the average Gaussian curvature is closer to zero and the lamellar phase results. Hence the three states are easily manipulated by varying the ratio of hexanol to CpCl.

These three states are easily distinguished by eye, thereby assisting in determining if a single equilibrated L_3 phase has been obtained. The lamellar phase has a very high viscosity, relative to both the L_3 and the reverse micelle phase. This phase is also less dense than the L_3 phase and birefringent. The L_3 phase is optically homogeneous, crystal clear and optically isotropic (indeed, it is difficult to distinguish from pure water). The presence of the second isotropic phase, the reverse micelle phase, is readily distinguished from the L_3 phase despite having low viscosity and appearing optically isotropic—when coexistent with the L_3 phase the resulting mixture is considerably turbid. Mixtures of coexisting phases may be pushed into the L_3 region by adding CpCl (in the case

(15) Roux, D.; Coulon, C.; Cates, M. E. *J. Phys. Chem.* **1992**, *96*, 4174−87.
    (16) Wennerström, H.; Olsson, U. *Langmuir* **1993**, *9*, 365−8.
    (17) Quilliet, C.; Blanc, C.; Kleman, M. *Phys. Rev. Lett.* **1996**, *77* (3), 522−5.
    (18) McGrath, K. M. *Langmuir* **1997**, *13* (7), 1987−95.

of the L_3 phase plus the second isotropic phase) or hexanol (in the case of the L_3 phase plus the lamellar phase). Equilibrated L_3 samples form within a day, although times may be considerably shorter for more dilute systems.[18]

Since the publication of our work on the L_3 phase templating, another novel approach has been reported on the synthesis of mesoscopic structures with pores as large as 30 nm through the use of amphiphilic triblock copolymers to direct the organization of silica to make hexagonal mesoporous silica.[19−23]

Experimental Section

Materials. Our L_3 structure is a thermodynamically stable phase composed of the surfactant cetylpyridinium chloride (CpCl, 1-hexadecylpyridinium chloride monohydrate, $C_{16}H_{33}(N^+)C_5H_5(Cl^-)\cdot H_2O$), the cosurfactant hexanol ($C_6H_{13}OH$, ca. 98% by gas chromatography), and hydrochloric acid (0.2 M, aqueous). This system was adapted from ref 18 by replacing the brine solution (aqueous NaCl) with dilute HCl (Figure 2). The source of chloride is immaterial. Varying amounts of the 0.2 mol dm^{-3} hydrochloric acid "solvent" were used to prepare samples, ranging from 50% up to 95% by weight of the overall mixture. A fixed ratio of approximately 1.15 (by weight) hexanol to CpCl[24] was used in all samples except at the high and low solvent composition limits of the L_3 phase (>90% or <60% by weight, respectively), which sometimes required some slight adjustment of the hexanol/surfactant ratio within the range of 1.12−1.20. The L_3 phase remains stable with respect to the solvent content throughout most of the solvent content range of interest, but the phase field narrows and curves upward when the solvent content exceeds 90% by weight (Figure 2).[18] Concomitant with an increase in solvent content is an increase in the pore diameter, as discussed below. The source of silica for silicification of the L_3 phase was typically tetramethoxysilane (TMOS).[25]

Synthesis of the Silicified L_3 Phase. The order of mixing of the three components of the L_3 system was not important to the final result, but it was necessary to maintain the correct hexanol/CpCl ratio to ensure phase purity and stability as stated above. Typically, to prepare a sample of the L_3 phase for this system, the CpCl and hexanol cosurfactants were mixed in an appropriate container to which the required amount of 0.2 mol dm^{-3} hydrochloric acid was then added. For example, to prepare 5 g of an L_3 phase containing 55 wt % solvent, the following amounts of materials were used: 1.0442 g of CpCl, 1.2489 g of hexanol, and 2.7506 g of 0.2 mol dm^{-3} HCl solution

(19) Zhao, D. Y.; Feng, J. L.; Huo, Q. S.; Melosh, N.; Federickson, G. H.; Chmelka, B. F.; Stucky, G. D. *Science* **1998**, *279* (5350), 548−52.
(20) Zhao, D. Y.; Yang, P. D.; Huo, Q. S.; Chmelka, B. F.; Stucky, G. D. *Curr. Opin. Solid State Mater. Sci.* **1998**, *3* (1) 111−21.
(21) Zhao, D. Y.; Huo, Q. S.; Feng, J. L.; Chmelka, B. F.; Stucky, G. D. *J. Am. Chem. Soc.* **1998**, *120* (24), 6024−36.
(22) Yang, P. D.; Zhao, D. Y.; Chmelka, B. F.; Stucky, G. D. *Chem. Mater.* **1998**, *10* (8), 2033.
(23) Zhao, D.; Yang, P.; Melosh, N.; Feng, J.; Chmelka, B. F.; Stucky, G. D. *Adv. Mater.* **1998**, *10* (16), 1380.
(24) In our original reference this was incorrectly printed as the "CpCl-to-hexanol" ratio.[14]
(25) Cetylpyridinium chloride was purchased from Sigma Chemical Co. and ICN Biomedicals, Inc. Hexanol was from Sigma Chemical Co. Sodium chloride (99.999% pure) was obtained from Aldrich Chemical Co. Ltd. Concentrated hydrochloric acid was standard chemical stores grade and was diluted to the appropriate concentrations. Water used was distilled deionized with conductivity between 1 and 10 MΩ cm. This source was used for all dilutions and preparation of solutions. Tetramethoxysilane (TMOS, $(CH_3O)_4Si$, ≥97% pure) and tetraethoxysilane (TEOS, $(CH_3CH_2O)_4Si$, ≥97% pure) from Alfa Aesar, Aldrich, and Fluka Chemica-BioChemika. Both TMOS and TEOS were checked for formation of condensate during storage prior to use. All chemicals were used as received.

(yielding a solution with h/c = 1.20 and solvent content of 54.5 wt %). Samples were equilibrated either by stirring using a magnetic stirrer or via agitation on a vortex mixer. Samples were held at room temperature, by using a water bath if necessary, during stirring. After 20−30 min of continuous stirring or repeated agitation cycles (agitating for a couple of minutes then allowing the sample to stand), the samples (except for solvent compositions of >90 wt %) became clear and would remain clear and optically homogeneous if set aside. Samples at solvent values of >90 wt % were optically homogeneous but very slightly turbid, possibly due to the formation of large pore diameter structures which scatter visible light. After being allowed to stand without stirring for several minutes, the samples were water clear, indicating that the L_3 phase was quickly established once agitation was removed. The only exceptions were the >90% solvent samples, which remained slightly turbid in appearance.

The L_3 liquids are stable with time and can be left to sit for several weeks if well sealed against the loss of solvent or hexanol. However, we found that surfactant solutions which were left for a period of months before silicate precursor were added had difficulty solidifying. Hence, as a precaution, surfactant solutions were made shortly before use. Once an optically homogeneous, single-phase sample was obtained, the phase would be "silicified" by the addition of a silicon alkoxide. To ensure complete hydrolysis of the alkoxide, the ratio of water to alkoxide was kept slightly greater (~4.25:1, molar) than the required stoichiometric ratio of 4:1 (molar). For example, 5.5 g of TMOS was added to a 5 g L_3 phase of 55 wt % solvent for a molar ratio of water to alkoxide of 4.22:1. TMOS was typically added *without* stirring to the L_3 phase solution as hydrolysis occurs sufficiently fast that mixing occurs during the addition.

Significant heat was generated by the immediate hydrolysis of the TMOS by the acidic solvent; adding TMOS too rapidly resulted in sample boiling and the concomitant loss of the volatile components. Temperatures of greater than 100 °C were reached when TMOS was simply poured into the L_3-phase-containing solution. To prevent rapid and uncontrolled heating, the alkoxide was added dropwise using a Pasteur pipet and the temperature of the solution was kept below 60 °C (e.g., below the boiling point of methanol, T_b = 64.5 °C).

After hydrolysis was complete (taken as the point at which the temperature of the sample returned to ambient), the samples were tightly sealed and set aside to gel. Samples would gel within 2−5 h after adding TMOS to the L_3-containing solution if incubated at 60 °C or usually within 48 h if held at room temperature. But the actual time required for a sample to gel increased with decreasing water content in the original solution. For example, for samples held at room temperature, we observed that materials prepared from 90 wt % solvent solutions would gel within 2 days, while those from a 55 wt % solution could take up to a week to gel. In all cases, the gelled samples were colorless and clear (again, as in the L_3 phase precursor samples, samples above approximately 90 wt % solvent appeared slightly turbid due to the light scattering effect of the characteristic spacing), optically isotropic, and assumed the shape of the container. The latter observation demonstrates the possibility of molding these materials into different forms as might be required. The gels could be strengthened by being kept at 60 °C for a week or more or merely by setting aside for longer times at room temperature.

Solvent Extraction. The resultant bulk, solid gels would still shrink considerably (with typical volume

reductions of more than 50%) if they were simply dried in air. Shrinkage could be almost completely eliminated by the use of various solvent extraction techniques: successive solvent extraction, Soxhlet extraction, and supercritical drying. Since the degree of shrinkage varied somewhat with the solvent extraction procedure, we chose to treat all samples for a given characterization study with a single extraction technique. Thus, all the samples used to determine the characteristic X-ray spacing (which is related to the pore size) were dried via successive solvent exchange.

X-ray characterization results discussed are for minimum shrinkage, taken to be "zero" point shrinkage (note that this was not physically measured in any other manner). Any shrinkage that did occur resulted in a reduced characteristic X-ray spacing (see below), since in effect the solvent composition had been decreased. This can be readily understood since for L_3 liquid crystalline phases the characteristic spacing scales with solvent volume fraction and any reduction of the solvent volume fraction will result in a reduction of the characteristic spacing. Indeed once a "zero" shrinkage scaling law was obtained, the amount of shrinkage for a particular sample could be estimated from this "calibration" curve. It should be noted that the characteristic spacing peak is a relatively weak diffraction feature and is most readily seen in dried gels because in these gels there is a large electron density contrast between the pore voids and the pore walls. The peak has not been seen in wet, as-prepared gels.

The successive solvent extraction procedure involves progressive and successive exchanges with various organic solvents. The first step was to exchange the water/methanol mixture for pure methanol by covering the sample with methanol shortly after the sample was gelled, that is, when the sample would no longer flow if the container was tilted or inverted. Samples in which the exchange process was begun as soon as they were gelled were observed to swell during the solvent exchange process during the later acetone exchange step, described below. Gels aged for another 24 h after gelation or prepared by heating at 60 °C were not observed to swell during solvent exchange. After several hours, the methanol would be poured off and replaced with fresh solvent. This process was repeated three or four times. The methanol-exchanged samples were then exchanged with increasingly rich acetone/methanol mixtures, starting with 10% acetone in methanol. The acetone fraction of subsequent washes would be increased by approximately 10% each time until pure acetone had been used as the wash three or four times. The last solvent used was acetic acid, in which the acetic acid in acetone fraction started at 10% and then increased by 10% steps. During the solvent exchange, the volume of the sample gel would not appear to change appreciably although internal fractures were often observed and the sample usually pulled away from the container walls during the acetic acid exchange step.

Even with the slow successive solvent exchange protocol, samples frequently fractured when the final acetic acid solvent was allowed to evaporate in air. This was particularly true when samples with large exposed surface-to-volume ratios were dried quickly. Fracture and shrinkage were minimized when the air-exposed surface to volume ratios were less than 10%. X-ray data were obtained for samples which were air-dried at room temperature after solvent exchange using samples prepared with surface-to-volume ratios of <10%. For these samples, shrinkage is estimated to be less than 5%. No intentional attempt was made to remove the surfactant; however, surfactant was partially removed by washing

out during the process of solvent exchange, as noted by the presence of surfactant in dried solvent washes.

As with other methods of sol−gel preparations, shrinkage remains a serious drawback in the formation and reproducibility of L_3 silicates. Strict compliance with solvent exchange was necessary to ensure that minimal shrinking was obtained. Samples which were simply air-dried over a period of 48 h after gelation would remain clear and monolithic with few cracks. However, final volumes were <50% of the initial, depending on the sample used, indicating a significant loss of pore volume. This loss was confirmed by X-ray scattering which often produced characteristic spacings of approximately 5 nm, indicating almost complete collapse of the silicate pore structure. Samples where the solvent exchange process was truncated after only methanol or after acetone exchange showed shrinkage similar to air-dried samples which were not solvent exchanged. Samples kept under liquid shrank more slowly and retained more of the original volume but remained fragile and very sensitive to subsequent handling and drying in air. When heated at temperatures above 100 °C, the samples invariably broke up into fragments (this was true for all samples, whether solvent exchanged or not). Longer curing times resulted in stronger samples, but shrinkage was still observed.

Continuous, Soxhlet extraction was sometimes used to remove the organic components, indicating the high connectivity of the pore network. The surfactant CpCl is soluble in water, ethanol, and methanol. Hexanol is only slightly miscible with water (8 parts per 100) but soluble in ethanol.[26] Solvents (including water, methanol, ethanol, acetone, THF, and *n*-heptane) chosen to cover a range of Hildebrand solubility parameters between 48.0 (water) and 15.3 MPa$^{1/2}$ (*n*-heptane) were used as extracting solvents. A sample of L_3 silicate would be placed in the extraction chamber of the Soxhlet extraction apparatus, cushioned on both sides by glass wool. A 500 mL boiling flask was half filled with solvent and heated to boiling. The distillation of the solvent resulted in a continuous stream of hot solvent flowing through the sample. Typical extraction runs lasted for four days. The extracted samples were allowed to air dry and then removed to a vacuum drying oven and held at 50 °C under vacuum. During drying, the samples invariably fractured into small pieces.

To prepare samples for transmission electron microscope (TEM) analysis, some samples were supercritically extracted using CO_2. Supercritical extraction (SCE) was done using a Milton Roy SCE Laboratory Methods Development System (Ivyland, PA), with runs averaging 8−10 h in duration. Samples to be extracted were placed in the extraction chamber after undergoing solvent exchange in acetone. The extraction chamber was sealed and slowly pressurized to >100 MPa and then heated to 40 °C. At the selected temperature and pressure, a shunt valve to a separation vessel was opened while supercritical conditions in the extraction chamber were maintained. Once pressures and temperatures in the extraction and separation vessels were equalized, a second shunt valve from the separation vessel to atmosphere was cracked to continuously vent CO_2 from the system, providing a continuous stream of extracting fluid passing through the sample. Extracted material was retained in the separation vessel.

Calcination. When required, samples were calcined in resistance-heated furnaces under air or oxygen-enriched atmospheres. A typical heating schedule consisted of (i)

(26) Dean, J. A. *Lange's Handbook of Chemistry,* 13th ed.; McGraw-Hill Book Co.: New York, 1985; p 7−437.

a slow ramp (5−10 °C/min) to 100 °C, (ii) dwell at 100 °C for 2 h, (iii) ramp to higher temperature (5−10 °C/min), (iv) dwell of varying duration at higher temperature, and (v) furnace cooled back to ambient. Samples were heat treated at 300 °C up to 30 h, at 500 °C for 2−4 h, and at 600 °C for no more than 2 h. Samples were invariably fractured by the furnace treatment into large granules ranging in size from 1 to 3 mm.

X-ray Diffraction. Small-angle X-ray Scattering (SAXS) was used to investigate the pore structure of dried, successive solvent-exchanged samples. Powder diffraction data for all samples prepared as described above were obtained using a Rigaku RU-200 rotating anode X-ray diffractometer (Danvers, MA) equipped with a microfocus cup. The generated Cu Kα X-rays were focused with bent mirror optics. Characteristic spacings ranging from 1 to 35 nm could be determined using these mirrors for the L_3 systems studied here. Two-dimensional X-ray images were collected with a home-built CCD detector based on a Thomson 512×512 pixel CCD,[27] thus enabling observation of any orientational effects within samples.

Digital powder diffraction images were azimuthally integrated to generate plots of scattered intensity versus $q = 4 \pi \sin \theta / 1.54$ Å, where 2θ is the angle between the incident and scattered beam directions used to obtain one-dimensional diffraction patterns. Samples either were flame sealed in glass X-ray capillaries of approximately 1.5 mm diameter (precursor, surfactant only, or L_3 phases) or consisted of chunks of silicified materials positioned on a U-shaped holder aligned with the incident beam. These latter samples were exposed to vacuum within the sample chamber, but over the time-scale of the experiment this had no apparent effect on completely dry samples.

Surface Area Measurements, Thermal Analysis, Electron Microscopy, and Atomic Force Microscopy. Surface area measurements were made on dried samples (with and without extraction) using a Micromeritics Flowsorb II 2300 single-point Brunauer, Emmett, and Teller (BET) gas-adsorption apparatus (Norcross, GA). Samples were air-dried, vacuum dried at 50 °C for at least 8 h, and then degassed at 100 °C under a flowing 70/30 He/N_2 gas mixture for several hours prior to measurement. Surface areas were determined from the amount of nitrogen gas adsorbed onto the silicate surfaces from a flowing stream of 70/30 He/N_2 gas at liquid nitrogen temperature (−196 °C).

Simultaneous differential scanning calorimetry (DSC) and thermogravimetric analysis (TGA) were performed using a Rheometrics STA1500 (Piscataway, NJ). Typical furnace runs were done under streaming air. The standard furnace run consisted of the following steps: (i) ramp from ambient to 600 °C at 5 deg/min; (ii) hold at 600 °C for 1 h; (iii) ramp at 20 °C/min back to ambient.

Scanning electron microscopy (SEM) was performed on air-dried samples mounted on graphite tape affixed to an aluminum mount. Samples were coated with carbon using a Cressington 208 carbon sputter coater (Cranberry, PA) to a uniform thickness between 150 and 300 Å. Imaging was performed using a Philips XL30 FEG-SEM (FEI Co., Hillsboro, OR) under a typical accelerating voltage of 15 kV.

High-resolution transmission electron microscope imaging and elemental analysis were performed using a Philips CM 200 field-emission TEM (FEI Co., Hillsboro, OR), operating at 120 keV, equipped with PGT-IMIX energy dispersive X-ray spectroscopy systems. Images

were obtained using air-dried, supercritically dried, and thermally treated samples of L_3 materials. TEM samples were prepared by microtoming slices from pellets composed of pieces of L_3 silicate mounted in epoxy (Spurr's kit, Electron Microscopy Sciences, Washington, PA). Observations were made on samples held at either ambient or liquid nitrogen temperatures, with no apparent variations in crystal structure observed between samples due to the temperature of analysis. Most of the high-resolution images shown here were collected at an imaging condition close to the Scherzer defocus at 120 keV. With the Schottky field emission gun, the TEM provides a probe less than 1 nm diameter with beam current around 500 pA, providing both X-ray and electron diffraction analyses at the subnanometer scale.

Atomic force microscope (AFM) imaging was performed with a Digital Instruments MultiMode scanning probe microscope (SPM) using the Nanoscope IIIa control system (Santa Barbara, CA).

Results and Discussion

The L_3 phase is characterized by a well-defined topology of bicontinuous pores with low polydispersity in the pore diameter, which yields a single, weak, broad X-ray scattering peak, called the characteristic spacing, superimposed on a monotonically falling background. The characteristic spacing of an L_3 phase is the average over the thickness of the bilayer plus the channel occupied by solvent (related to the characteristic pore diameter). It is a broad peak because it is the average of all chords across the randomly oriented channels. Some of these chords are perpendicular to the pore walls; others happen to be oriented at glancing angles to the walls and, therefore, are of longer lengths even if the pore diameter is constant.

It is normally quite difficult to measure the weak SAXS from L_3 phases with large characteristic spacings because the signal gets lost in the camera background near the primary beam stop. In addition to the desired SAXS peak, the silicate materials also show enhanced low-angle background, which even further reduces the relative intensity of the characteristic spacing peak. These backgrounds may be distinguished from the characteristic peak in that their intensity falls off monotonically with increasing angle. With our X-ray apparatus, the background restricted the observable data to samples with solvent fraction below ∼90 wt %, corresponding to a repeat distance of ∼35 nm.

A remarkable feature of these materials is that in some samples (but not all!), powdering the samples caused the SAXS peak to disappear or shift in position. The straightforward conclusion is that powdering the samples resulted in catastrophic disintegration down to nanometer levels. We find this explanation difficult to accept, but we have been as yet unable to develop a more suitable interpretation of the changes in the diffraction pattern following crushing or grinding.

Figure 3 shows the one-dimensional diffraction patterns for a liquid crystalline L_3 phase and a silicified L_3 phase. The silicified phases used to produce the "zero" point dilution curve shown in Figure 4 were those that had been synthesized at room temperature with surface-to-volume ratios of <10%, successively solvent-exchanged and air-dried. Samples were not heated and no attempt to remove surfactant or cosurfactant had been made. Both silicified and precursor L_3 phases show a broad band diffraction peak, which is superimposed upon a large wide-ranging small-angle scattering background. The broadness of the peak is in part due to the random pore structure; that is,

(27) Tate, M. W.; Gruner, S. M.; Eikenberry, E. F. *Rev. Sci. Instrum.* **1997**, *68* (1), 47−54.
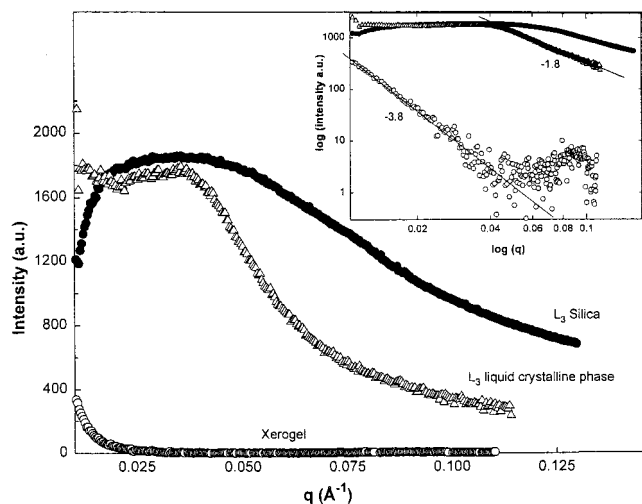
Figure 3. One-dimensional diffraction patterns for a xerogel (○), a liquid crystalline L_3 phase (55 vol %, △), and a silicified L_3 phase (●). The liquid crystalline L_3 phase has a limiting behavior dependence of $q^{-1.8}$ (inset), correlating to a local bilayer structure. The silicified L_3 phase should exhibit this same asymptotic behavior if the topologies are similar. Although experimental limitations hinder exact determination, a limiting behavior of q^{-2} is indicated for the L_3 silicate (inset). For an xerogel formed without surfactant, there is no peak and the limiting behavior decays as $q^{-3.8}$ (inset).[14]
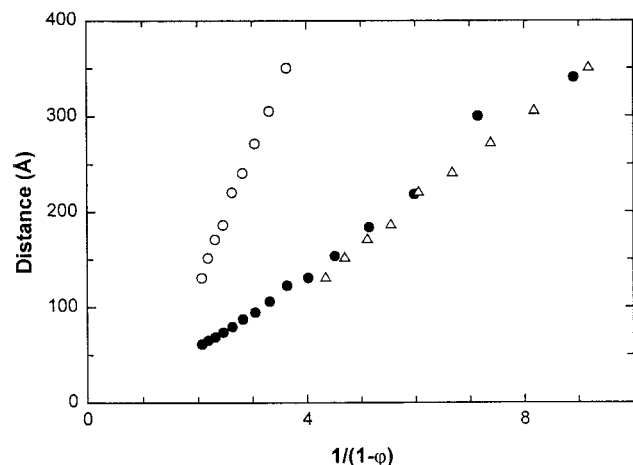
Figure 4. Dilution law determined at 20 °C for the liquid crystalline L_3 phase (●) and the silicified material (○, △). If we ignore the effect of diluting the solution with methanol from the hydrolysis of the TMOS (○), the two scaling laws do not coincide. However, when this is taken into consideration (△) there is complete correlation between the liquid crystalline phase and the silicified material, indicating that the respective underlying topologies coincide.[14]

it results from the ensemble average of chord lengths that vary in size because they strike across the pores at random.

A characteristic spacing for the phase may be obtained via a tangential base line method. This characteristic spacing is related to the pore diameter and can be varied by changing the solvent content in the template solution. The linear relationship between the solvent fraction and the characteristic spacing is discussed below. The limiting dependence of the intensity as a function of the reciprocal lattice vector may be used to determine the spatial dimension of the clusters, which is the parameter required to specify the fractal network dynamics; as such it is often called the fractal dimension (i.e., the intensity decreases as $I \propto q^{-D}$, assuming monodispersity of both particles and
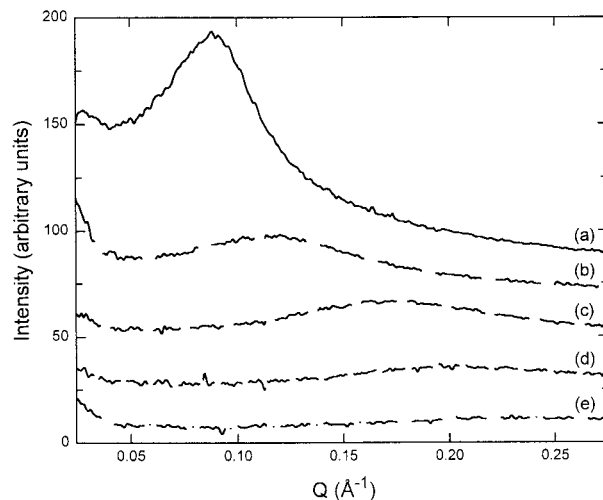

Figure 5. Small angle X-ray scattering pattern for a 60 wt % total solvent surfactant-only L_3 phase solution with methanol concentrations of (a) 0%, (b) 25%, (c) 50%, (d) 65%, and (e) 75% of the total solvent concentration. The pattern at 65% methanol corresponds to the concentration of methanol in a typical silicate L_3 synthesis, once hydrolysis of the added TMOS is complete. The patterns are offset vertically for clarity.

clusters[28]). A relation between the power-law exponent and the fractal dimension can only be given if the cluster size distribution obeys a power law[29] and the aggregates are self-similar (such as is the case for the L_3 phase).[30] The inset to Figure 3 shows the double-logarithmic representation of the one-dimensional scattering patterns. The characteristics of the diffraction pattern can be related to the different structural features correlated with the respective length scale. At the lowest q values, the scattered intensity is constant since at the corresponding large length scales, scattering does not allow resolution of the inhomogeneities of the sample.

The intermediate dependence can be explained in terms of fractals. Smooth surfaces (e.g., colloidal aggregates, such as those in *some* aerogels and xerogels) decay as q^{-4} following Porod's law, whereas bilayer structures as in the case of the liquid crystalline L_3 phase (and lamellar phases) follow a q^{-2} dependence. The liquid crystalline L_3 phase (a 55 wt % sample) has a limiting behavior dependence of $q^{-1.8}$, which within experimental uncertainty correlates with a local bilayer structure as expected. If the silicified L_3 phase conforms to the topology of a liquid crystalline L_3 phase, it too must show this asymptotic behavior. Due to the increased broadness, reduced intensity, and long tail of the diffraction peak of the silicified L_3 phases, determining the true asymptotic behavior was hindered by the experimental limit of our diffraction camera. However, all indications lead to a limiting behavior of q^{-2} rather than q^{-4} as observed in some aerogels and xerogels. Figure 3 also shows the small-angle diffraction data for a silicate gel formed via traditional xerogel methods (i.e., without surfactant): no peak is apparent and the limiting behavior decays as $q^{-3.8}$, as expected for a cross-linked network of smooth spheroidal particles.

In order to analyze the diffraction data in a reproducible and quantitative manner the volume fraction of solvent must be known. Liquid crystalline L_3 phases, upon dilution, follow a universal scaling law.[18] Such systems

(28) Teixeira, J. In *On growth and form*; Stanley, H. E., Ostrowshy, N., Eds.; Nijhoff: Dordrecht, 1986; p 145.
(29) Martin, J. E. *J. Appl. Cryst.* **1986**, *19*, 25.
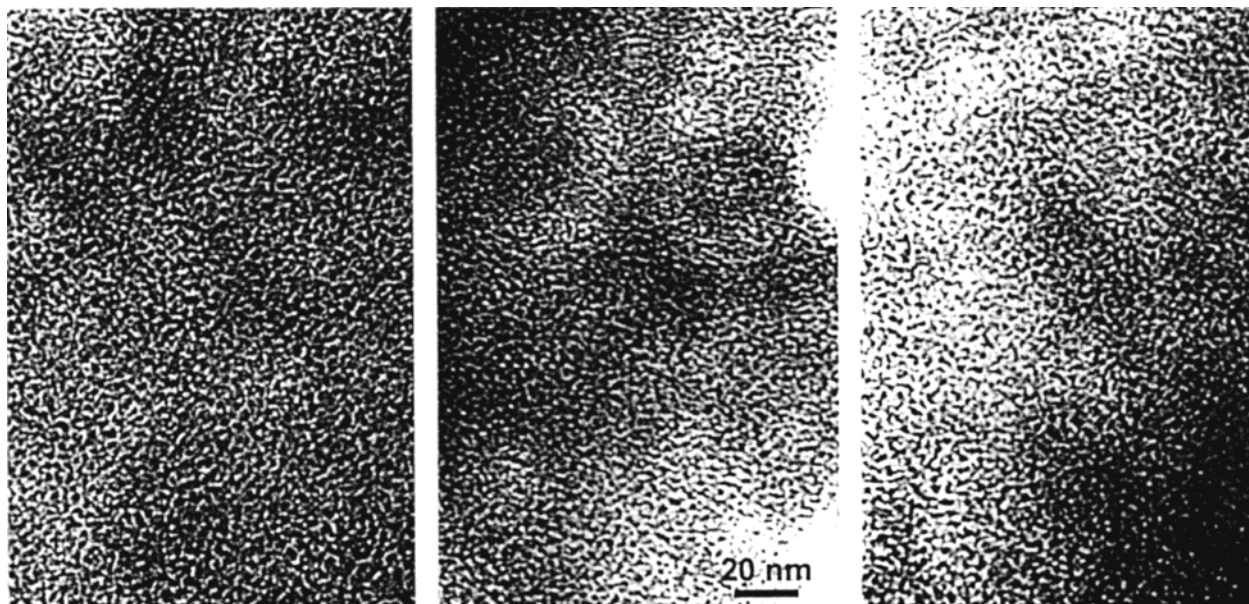(30) Schaefer, D. W. *Science* **1989**, *243*, 1023.

Figure 6. TEM images: (a) as prepared L_3 silicate, air-dried; (b) supercritically dried silicate, and (c) supercritically dried then heat treated at 600 °C for 1 h. The apparent structure does not appear to be affected by low-temperature drying and/or extraction. Measured surface areas in supercritically dried samples were higher than those in air-dried samples ($\sim$600 m^2 g^{-1} as opposed to $\sim$400 m^2 g) but were still higher in the heat-treated samples (>900 m^2 g^{-1}).
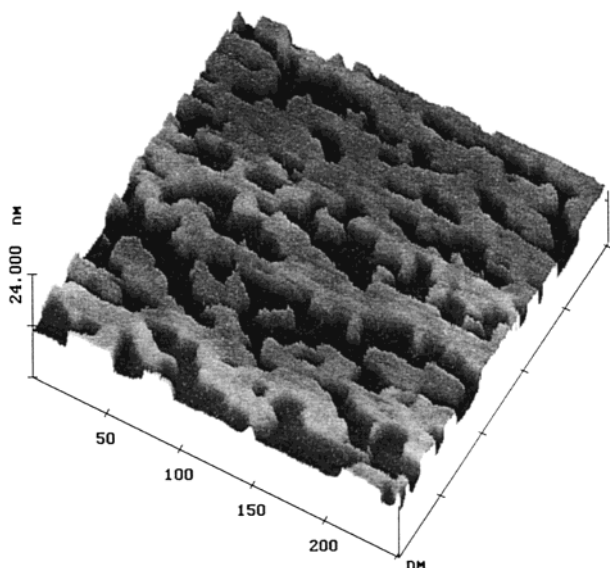
Figure 7. AFM image of L_3 silicate film on glass substrate showing channels and walls at the surface of the film. After adding TMOS to the L_3 solution, the sample was allowed to stand at room temperature for 24 h, which resulted in a thickened solution suitable for spin coating. The film was cured at 60 °C overnight but was not extracted prior to characterization. Tapping mode AFM was used to image the surface.

are termed self-similar, appearing identical at all length scales. For a system to follow a universal scaling law the topological form of the phase must remain unchanged upon dilution (i.e., pure swelling alone occurs) and the characteristic distance increases linearly as a function of the reciprocal of the solvent volume fraction. Hence increasing or decreasing the amount of solvent relative to the surfactant/cosurfactant content merely results in a change in the characteristic spacing (thus changing the pore diameter), under the restriction that any variation in the volume fraction of the solvent does not push the system into a different phase field. For the L_3 phase studied here these boundaries lie between volume fractions of $\sim$53 to >99 wt % solvent.

Analysis of the silicified L_3 phases was complicated by the large increase in volume fraction upon addition of the silicate precursor and also due to shrinkage (reduction of the solvent volume fraction) subsequent to gelation and drying. Assuming "zero" shrinkage occurs when the sample is prepared as previously described, an upper volume fraction limit may be determined from the densities of the TMOS (added precursor) and methanol (byproduct). Characteristic spacings were found to decrease depending on the extent of shrinkage. As discussed above, care was taken to treat all samples in an identical manner in order to limit variations in shrinkage and the consequent volume fraction. X-ray data obtained at such samples produced characteristic distances which corresponded to limiting volume fractions. The characteristic distances obtained in this fashion are shown in Figure 4.

Once the "zero" point universal scaling law had been obtained it was possible to determine the extent of shrinkage for other samples which had not been treated in the same manner, since the zero point curve could be used as a calibration curve. This follows as shrinkage has the consequence of concentrating the phase (i.e., through a reduction of the solvent volume fraction). The silicate walls of the network begin to crack as shrinking continues since the walls of the structure are now amorphous silica and rigid. In addition to a maximum volume fraction due to the amounts of aqueous HCl, silicate and methanol that were appropriate for the sample in question, a minimum volume fraction corresponding to the total shrinkage (as shrinkage is proportional to the extent of solvent removal) depends on the mechanism of drying and the extent of condensation within the silicate walls at the point drying began. A minimum diffraction peak corresponding to a repeat distance of $\sim$4.5 nm was obtained across all solvent volume fractions studied which correlates with a wall composed of the surfactant bilayer and polymerized silica alone.

The result of the L_3-silicate synthesis procedure is very sensitive to the exact synthesis conditions. A plausible reason for this sensitivity is illustrated by Figure 5, which shows the diffraction profile for surfactant-only L_3 phases (i.e., with no added silicate precursors) at fixed solvent
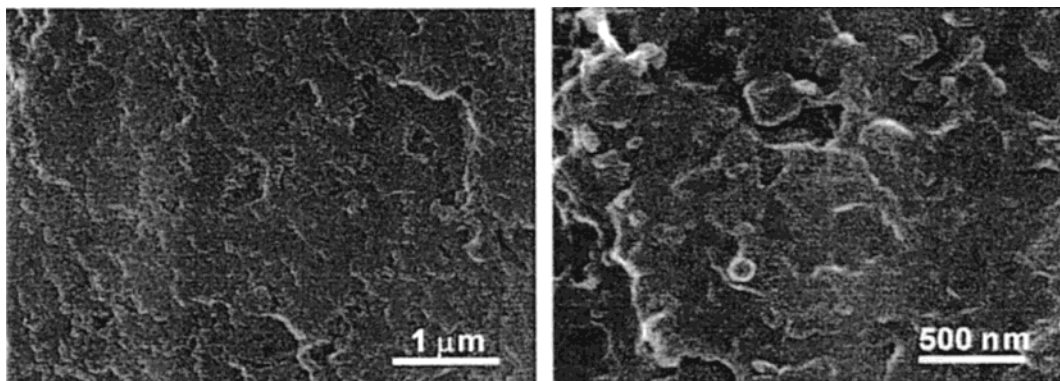
Figure 8. SEM of L$_3$ silicate monoliths, freeze fractured surface.

volume fraction for different methanol concentrations. It should be noted that the characteristic peak broadens and moves to higher Q (or smaller d-spacing) with increasing methanol, demonstrating that the L$_3$-phase structure varies as the methanol concentration changes. Since methanol is a product of TMOS hydrolysis, it can be expected that the L$_3$ structure in the presence of the silica precursor is also sensitive to the methanol concentration, and the structure of the final gelled product will depend on a competition between the respective rates at which (i) hydrolysis is producing methanol and (ii) condensation is "locking in" the resultant structure. Small perturbations in these two rates may cause the gel to freeze in different structures or, even worse, create a variety of structures within the same monolith. This suggests that a more robust synthesis would result if the synthesis were somehow modified to either allow complete hydrolysis before condensation begins or to yield byproducts that would not change the basic L$_3$ phase structure.

The continuity of the pore network is confirmed by transmission electron microscopy and atomic force microscopy. We have observed that the structure formed by the silicified L$_3$ material is highly uniform, with apparently high degrees of continuity and contiguity in the pore structure and the network walls (Figure 6). As previously reported, two-point pair-correlation function analysis performed on the dried silicate L$_3$ material showed that at distances above approximately 2.5 nm the system is completely random,[14] indicating no larger well-defined length scale and no longer-range correlation, within the sample. Estimated pore size for the dried sample shown in Figure 6 correlates to approximately 6 nm. AFM imaging (Figure 7) on a 75% solvent (v/v) material allowed to air dry and then cured at 60 °C overnight further supports the proposed topography of the L$_3$ silicate. As is readily apparent, the structure consists of two interpenetrating networks of solid and void, suggested by both SAXS and TEM analysis. A representative SEM images of an L$_3$ monolith is shown in Figure 8. The appearance of the monolith is very similar to that of a porous aerogel, indicating the isotropic structure in the silicate solid.

An advantage for a material with a well-defined and continuous pore structure is effective mass transport, both in infiltrating the matrix or when removing materials from the matrix. As shown in Figure 6, there is little apparent change in the structure of the silicate whether air-dried, supercritically dried, or supercritically dried and then heat treated at 600 °C for 1 h. In spite of the similarity of structures, samples heat treated at 600 °C range in color from clear to black. The coloration is due to the retention of organic residues or carbon within the matrix and is related to extraction of the sample prior to heat treatment. As shown in Figure 9a, the CpCl surfactant readily oxidizes
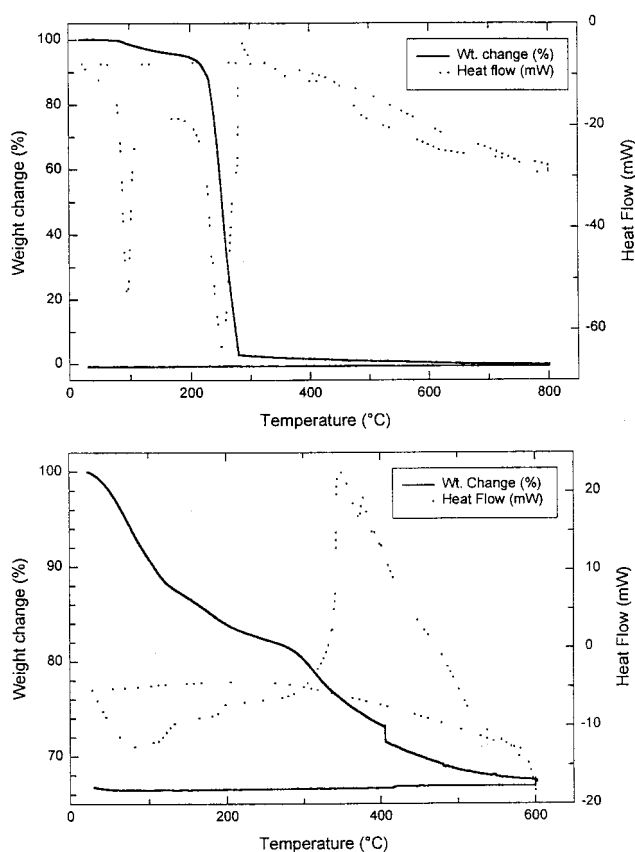

Figure 9. (a) Thermal decomposition of the surfactant cetylpyridinium chloride (CpCl) in air. (b) Thermal decomposition profile of a dried L$_3$ monolith in air.

in air before 300 °C. In the as-made L$_3$ gel, the degradation of the surfactant is slowed by the silica matrix (Figure 9b), with a more complex burnout. As the silicate is heated up to 200 °C, the more volatile components of the gel (water, methanol, and hexanol) are removed from the matrix. As the temperature approaches 300 °C, the CpCl surfactant begins to decompose. The decomposition of the surfactant is slowed by the presence of the silica wall encompassing the surfactant (Figure 1). Overall wall porosity may be the governing factor in the retention of the organic, and defects in the pore network could result in dense regions wherein organic material is trapped and cannot be simply removed. By 600 °C most of the organic material would be expected to be have been decomposed, but in some samples sufficient retained carbon colors the material.

Measured surface areas in as-made samples indicate only a moderate variation in surface areas across the range
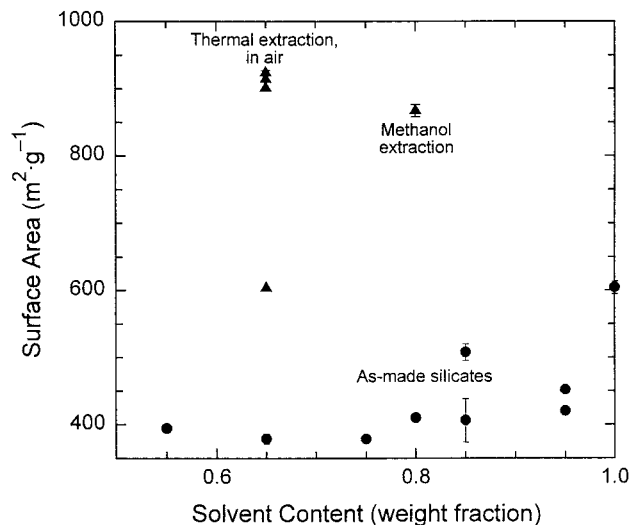
Figure 10. Single point surface area measurements on dried and extracted L_3 silicate monoliths. Air-dried, as-made monoliths have comparable surface areas across the range of solvent fractions. However, simple thermal or solvent extractions of the monolith are sufficient to dramatically increase the available surface area, possibly indicating that the interwall spacing between the silica layers (Figure 1) are opened by the extraction process.
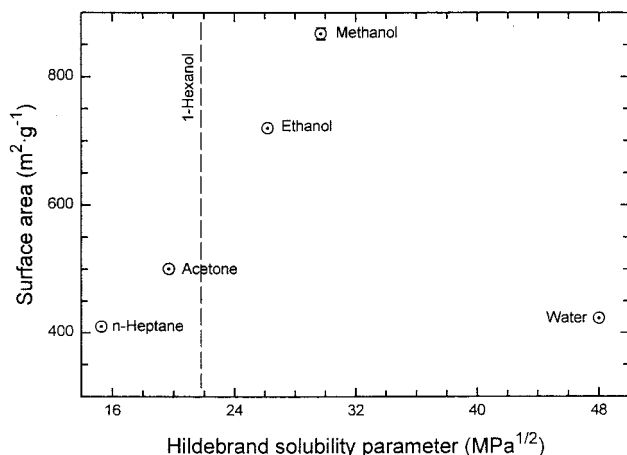

Figure 11. Effectiveness of Soxhlet extraction of L_3 silicates by solvent. The increase in measured surface area with increasing CpCl solubility is a strong indication that the structure of the silicate is open and permits fairly rapid solvent exchange within the matrix.

of solvent fractions (Figure 10), with observed areas lying between 375 and 500 $m^2\,g^{-1}$. For comparison, simple silica gels formed without surfactants but using comparable amounts of TMOS in 0.2 M HCl yielded surface areas around 600 $m^2\,g^{-1}$. However, when heated to 600 °C, measured surface areas in the L_3 silicate rise to more than 900 $m^2\,g^{-1}$, whereas in a simple gel surface is lost due to pore collapse and wall sintering. The change in surface area confirms the TEM observations that the structure of the L_3 gel is unaffected by low-temperature heat treatments while also demonstrating the enhancement in surface area by simple pyrolysis of the organic component.

If simple solvent extraction is used either before or in lieu of heat treatment, the behavior of the gel again indicates the openness of the structure. In Figure 11, the effect of different solvents on the measured surface area
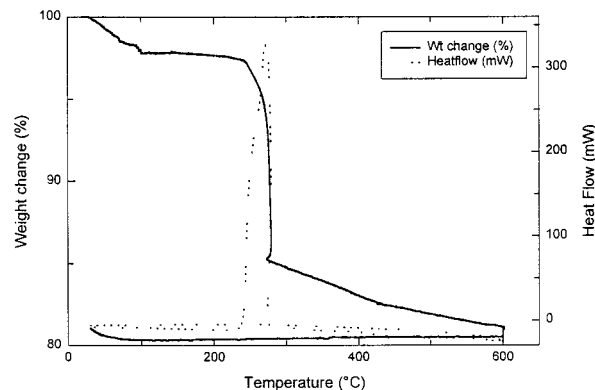

Figure 12. Thermal profile of methanol-extracted L_3 monolith. The rapid decomposition of the remaining organic is very similar to that of the CpCl surfactant in air (Figure 9a). Heat treating methanol-extracted samples to either 350 or 600 °C resulted in optically clear materials of comparable surface areas.

of the resulting silicate is shown as a function of the Hildebrand solubility parameter of the respective solvents.[26] Methanol, which is produced as a byproduct of the TMOS hydrolysis, results in surface areas nearly comparable to simple heat treatments, implying that simple solvent extraction also results in the removal of a significant portion of the organic material from the matrix. Thermal analysis of methanol-extracted samples (Figure 12) demonstrates the effectiveness of the solvent extraction on the structure. The thermal profile resembles the pyrolysis of the surfactant in air (Figure 9a) in both the onset of pyrolysis and the rapidity with which mass is lost. Although some organic debris is retained (apparent in the continuing weight loss tail at temperatures above 300 °C), the resulting materials are optically clear and colorless. We have not determined if the increase in effective surface area is due to further opening the pore network through extraction of byproducts, by removing the surfactant and hexanol between the silica layers (Figure 1), or some combination of the two processes.

Conclusions

Monolithic and thin film forms of a silicate consistent with the L_3 phase of lyotropic liquid crystals have been synthesized. Measured surface areas range from 400 $m^2\,g^{-1}$ in the dried gel up to >900 $m^2\,g^{-1}$ in simply extracted monoliths. SAXS, TEM, and AFM observations confirm the isotropic structure of the silicates across solvent contents ranging from 55% up to 95% by volume. The relative ease with which most of the organic phase can be removed from the silicate strongly suggests that pore connectivity and contiguity remain high in these materials. Although under normal drying conditions these silicates fracture into small pieces, it is anticipated that this problem will be eliminated through supercritical extraction of the solvent.